Corrosion Science 66 (2013) 369–379

Contents lists available at SciVerse ScienceDirect

Corrosion Science

journal homepage: www.elsevier.com/locate/corsci

Corrosion behavior of Alloy 690 in aerated supercritical water

Xiangyu Zhong, En-Hou Han *, Xinqiang Wu *

State Key Laboratory for Corrosion and Protection, Institute of Metal Research, Chinese Academy of Sciences, Shenyang 110016, PR China
Liaoning Key Laboratory for Safety and Assessment Technique of Nuclear Materials, Institute of Metal Research, Chinese Academy of Sciences, Shenyang 110016, PR China

ARTICLE INFO

Article history:
Received 3 August 2012
Accepted 1 October 2012
Available online 10 October 2012

Keywords:
A. Alloy
B. SEM
B. XPS
C. High Temperature Corrosion
C. Oxidation

ABSTRACT

The oxidation behavior of Alloy 690 exposed to aerated supercritical water at different temperatures was investigated using gravimetry, scanning electron microscopy/energy dispersive X-ray spectroscopy, X-ray diffraction, X-ray photoelectron spectroscopy, Raman spectroscopy and electron probe micro-analyzer. The oxide films showed a duplex layer structure with Ni and Fe rich in the outer layer, and Cr rich in the inner layer. Some pits and nodules observed in the oxide films could be related to TiN inclusions in the alloy matrix. The oxidation mechanism and effects of TiN inclusions are discussed.

1. Introduction

Supercritical water cooled reactor (SCWR) is one of the most promising advanced reactor concepts for Generation IV nuclear reactors because of its high thermal efficiency and plant simplification [1,2]. For the safety of the nuclear power plant, the corrosion behavior of candidate materials used in such an aggressive environment needs to be understood. Nickel-based alloys have been considered as one kind of candidate materials for SCWR due to their combined good corrosion resistance and mechanical properties in high temperature and high pressure water [3–5]. Many nickel-based alloys such as Alloy 625, Alloy 617, Alloy 718 and Hastelloy C-276 have been investigated as candidate materials for SCW systems [5–9]. The corrosion behavior of Inconel 625 exposed to a deaerated SCW in a temperature range of 400–550 °C showed fluctuations in weight change measurements and pitting as the predominant corrosion mode, and it was assumed that the fluctuations of weight change were related to the pitting and spalling [7,10]. While other authors found that a weight gain appeared for Alloy 625 exposed to SCW contains H_2O_2 and C-276 exposed to deareated SCW [8,9]. Microstructure often plays a leading role in corrosion resistance [10]. The γ′-phase such as $Ni_3(Al, Ti)$ is a common intermetallic precipitate in Nickel-based alloys, the carbides $M_{23}C_6$ in the grain boundary have strong influence on the resistance to intergranular corrosion and stress corrosion cracking [11–13], and the TiN inclusions act as the initiation sites of pitting [14,15], corrosion fatigue [16] and stress corrosion cracking [17]. The TiN inclusions oxidized much faster than metal matrix and resulted in high shear strain in the oxide scales, leading to the shrinking and cracking of the oxide films [18]. Therefore, these inclusions have a strong influence on the corrosion behavior of nickel-based alloys in SCW, and the effects of the inclusions need to be further investigated.

The present work is to investigate the corrosion behavior of Alloy 690 exposed to aerated SCW with different temperature and time, and to characterize the phase composition, morphologies and chemical composition of the oxide films formed on the surface of Alloy 690. The related corrosion mechanism and the effects of TiN inclusions are also discussed.

2. Experimental

2.1. Apparatus

Exposure tests were performed with a continuous flowing SCW system consisting of an HPLC pump (Eldex Inc., AA-100-S), a preheater, a nickel-based Alloy 625 autoclave with a volume of 850 ml, a heat exchanger and a back-pressure regulator (BPR) (Fig. 1). The internal pressure was measured by a pressure sensor placed at the inlet of the reactor and controlled by an HPLC pump and a BPR. A computer with Labview 6.0 software was used to control the internal pressure and the temperature in autoclave and preheater was monitored by two thermocouples. The test solution was aerated pure water with 8 ppm (by weight) O_2, and the flow rate was maintained at 5 ml/min.

* Corresponding authors at: State Key Laboratory for Corrosion and Protection, Institute of Metal Research, Chinese Academy of Sciences, 62 Wencui Road, Shenyang 110016, PR China. Tel.: +86 24 2384 1883; fax: +86 24 2389 4149.
E-mail addresses: ehhan@imr.ac.cn (E.-H. Han), xqwu@imr.ac.cn (X. Wu).

0010-938X/$ - see front matter © 2012 Elsevier Ltd. All rights reserved.
http://dx.doi.org/10.1016/j.corsci.2012.10.001

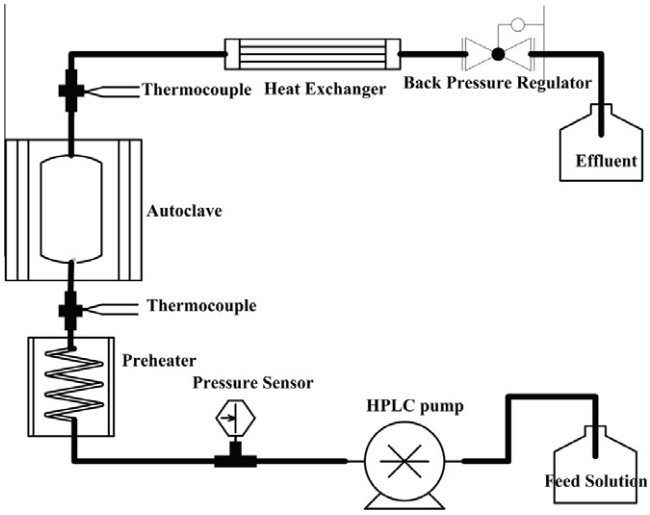

Fig. 1. Schematic diagram of supercritical water experimental apparatus.

2.2. Materials and specimens

Alloy 690 used in the present work was solution annealed at 1333 K for 0.5 h and then water quenched. Table 1 is the chemical composition of the alloy. Fig. 2a and b are the metallographic images of the as received alloy. The microstructure of the alloy is typical austenite with many annealing twins (Fig. 2a) and TiN inclusions were clearly observed in the alloy (Fig. 2b). Specimens (10 mm × 12.5 mm × 2 mm) for expose test in SCW were mechanically ground progressively with fine grit silicon-carbide paper up to 2000# grit, and final mechanical polished with 2.5 μm diamond paste. Prior to each test, the specimens were cleaned with ethanol and ultrasonically rinsed with deionized water for 30 min.

2.3. Methodology

The specimens were mounted on a rack and put into the autoclave. The testing conditions were maintained at 450 °C/25 MPa and 550 °C/25 MPa and the exposure time was up to 500 h. After exposure test, the specimens were cleaned with deionized water and dried. Then they were characterized by weight gain measurement, surface analysis and cross-section analysis. The weight of all specimens before and after exposure was measured using Sartorius BP211D microbalance with a resolution of 10^{-5} g. Corrosion products analysis were performed by D/Max 2400 X-ray diffractometer (XRD) using copper radiation (λ = 1.542 Å) and a BWS905 custom Raman system. The Raman system contains a powerful laser at 532 nm with a maximum power of 1.5 W. The Raman shift range is 175–2875 cm^{-1} and the spectral resolution is 12 cm^{-1}. The integration time used was 15 or 20 s depending on the signal intensity of the specimens. The surface and cross-section morphologies and compositions of oxide films were performed using scanning electron microscopy (SEM) (FEI INSPECT F50) equipped with an energy-dispersive X-ray spectroscopy (EDS) system. To investigate the cross-sections of the oxide films, some specimens were coated in Ni–P solution to protect the films. The coated specimens were mounted with epoxy resin and then polished. The corresponding cross-sections of the oxide films were examined using SEM and EDS. An electron probe micro-analyzer (EPMA-6010) was used to detect the distribution of O, Ni, Cr and Fe elements on cross-section under the operating condition of U = 15 kV and I = 100 nA. X-ray photoelectron spectroscopy (XPS) measurements were performed with ESCALAB250 X-ray photoelectron spectrometer. Photoelectron emission was excited by monochromatic Al Ka source operated at 150 W with initial photo energy 1486.6 eV. The C1s peak from adventitious carbon at 285 eV was used as a reference to correct the charging shifts. Depth profile information was performed over an area of 2 × 2 mm^2 under 2 keV Ar-ion sputtering and spectra were obtained over a 0.5 mm spot using a focusing X-ray monochromator. Sputtering rate was determined to be about 0.2 nm/s (vs. Ta_2O_5). The peak decomposition of the species in the oxide films was carried out with a commercial peak fitting software (XPSpeak4.1) using Gaussian–Lorentzian peak fitting after Savitzky–Golay smoothing and Shirley background subtraction, and the peak areas were converted to atomic concentrations as depending on sputtering depth.

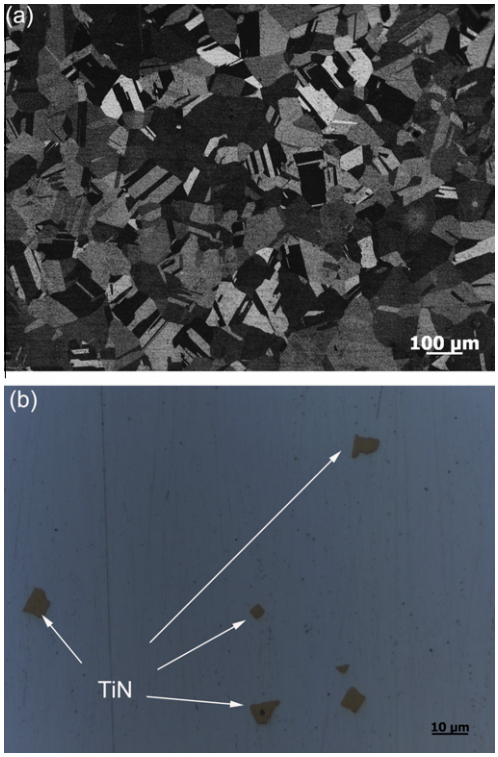

Fig. 2. (a) The metallographic image of as received Alloy 690, (b) light optical morphologies of the TiN on Alloy 690 surface.

3. Results

3.1. Gravimetry

Fig. 3 shows the weight gain of Alloy 690 exposed to SCW at 450 °C/25 MPa and 550 °C/25 MPa for different times. The weight gain of Alloy 690 at 550 °C is higher than that at 450 °C, and the trend of the weight gain at 550 °C is different from that at

Table 1
Chemical compositions of Alloy 690 (wt.%).

C	N	Cr	Fe	Mn	P	Si	Al	Ti	Cu	Nb	Co	Ni
0.013	0.01	29.15	9.19	0.21	0.01	0.02	0.26	0.305	0.01	0.01	0.01	Bal